

SPH model for stochastic Navier-Stokes and advection-diffusion equations

Jannes Kordilla
University of Göttingen
Dept. Applied Geosciences
Göttingen, Germany
jkordil@gwdg.de

Alexandre Tartakovsky, Wenxiao Pan
Pacific Northwest National Laboratory
Computational Mathematics Group
Richland, USA

Abstract—We propose a novel Smoothed Particle Hydrodynamics (SPH) discretization of the fully-coupled Landau-Lifshitz-Navier-Stokes (LLNS) and advection-diffusion equations. The accuracy of the SPH solution of the LLNS equations is demonstrated by comparing the scaling of velocity variance and self-diffusion coefficient with kinetic temperature and particle mass obtained from the SPH simulations and analytical solutions. To validate the accuracy of the SPH method for the coupled LLNS and advection-diffusion equations, we simulate the interface between two miscible fluids. We study the formation of the so-called giant fluctuations of the front between light and heavy fluids with and without gravity, where the light fluid lays on the top of the heavy fluid. We find that the power spectra of the simulated concentration field is in good agreement with the experiments and analytical solutions. In the absence of gravity the power spectra decays as the power -4 of the wave number except for small wave numbers which diverge from this power law behavior due to the effect of finite domain size. Gravity suppresses the fluctuations resulting in the much weaker dependence of the power spectra on the wave number. Finally the model is used to study the effect of thermal fluctuation on the Rayleigh-Taylor instability.

I. INTRODUCTION

In the presence of a macroscopic concentration gradient (e.g. the concentration gradient across the front separating two miscible fluids), non-equilibrium systems are known to relax to an equilibrated state via diffusion [1]. On macroscopic scales diffusion is often approximated by Fick's law [2]. However, on mesoscopic or molecular scales thermal fluctuations become a significant part of the hydrodynamics and greatly influence mixing. Thermal fluctuations may have a significant impact on miscible fluids close to a hydrodynamic instability such as Rayleigh-Taylor and Kelvin-Helmholtz instabilities. For example, thermal fluctuations produce anomalously large fluctuations of the front separating two miscible fluids (with a light fluid overlaying a heavy fluid, [3]).

To capture the effect of thermal fluctuations on the fluid flow on the hydrodynamic scale, [4] proposed a stochastic form of the Navier-Stokes equations that is commonly referred to as the Landau-Lifshitz-Navier-Stokes (LLNS) equations. In the LLNS equations, a random stress is added to the Navier-Stokes equations, and the strength of the random stress is related to the viscous stress via the fluctuation-dissipation theorem.

Similarly, a random mass flux is added into the advection-diffusion equation to consistently include the effect of thermal fluctuations on Fickian diffusion. The most common numerical techniques for directly solving the LLNS and stochastic diffusion equations are based on the finite-volume method [5]. Stochastic Lattice-Boltzmann models [6] and smoothed dissipative particle dynamics (SDPD) [7] have been used to model fluid flow in the presence of fluctuations, but these methods have not been derived via the direct discretization of the LLNS equations. For example, SDPD is obtained by adding a random force into the SPH discretization of the (deterministic) NS equations, and relating the magnitude of the random force to the viscous SPH force via the GENERIC framework [8].

Here we use the SPH method to solve stochastic partial differential equations including the LLNS and advection-diffusion equations. With regard to the LLNS equations, the SPH discretization provides an alternative to SDPD for introducing fluctuations in the SPH flow equations. It also provides a consistent framework for discretizing other stochastic conservation equations. The accuracy of the solution of the stochastic diffusion equation is verified by comparing moments of a conservative tracer with the analytical solution. Finally, we use the coupled LLNS and advection-diffusion equations to study the effect of fluctuations on the diffusive front in the absence and presence of gravity. We analyze the spatial correlation of the diffusive front geometry and compare the results with the theoretical predictions. Furthermore the classical Rayleigh-Taylor instability is simulated to verify the accuracy of the stochastic SPH model.

II. STOCHASTIC FLOW AND TRANSPORT EQUATIONS

We study the isothermal stochastic Navier-Stokes equations including the continuity equation

$$\frac{D\rho}{Dt} = -\rho(\nabla \cdot \mathbf{v}), \quad (1)$$

the stochastic momentum conservation equation

$$\frac{D\mathbf{v}}{Dt} = -\frac{1}{\rho}\nabla P + \frac{1}{\rho}\nabla \cdot \boldsymbol{\tau} + \mathbf{g} + \frac{1}{\rho}\nabla \cdot \mathbf{s} \quad (2)$$

and the advection-diffusion equation

$$\frac{DC}{Dt} = \frac{1}{\rho} \nabla \cdot (\rho D^F \nabla C). \quad (3)$$

Here $D/Dt = \partial/\partial t + \mathbf{v} \cdot \nabla$ is the total derivative and ρ , \mathbf{v} , P and \mathbf{g} are the density, velocity, pressure and body force, and D^F is the Fickian diffusion coefficient. The components of the viscous stress $\boldsymbol{\tau}$ are given by

$$\tau^{ik} = \mu \left(\frac{\partial v^i}{\partial x^k} + \frac{\partial v^k}{\partial x^i} \right), \quad (4)$$

where μ is the (shear) viscosity and the bulk viscosity is assumed to be equal to $\frac{2}{3}\mu$. $C = \tilde{C}/C_{max}$ is the normalized mass fraction of solute varying from zero to one (\tilde{C} is the mass fraction and C_{max} is the maximum mass fraction). In the following, we refer to C as concentration. The fluctuations in velocity and concentration are caused by the random stress tensor

$$\mathbf{s} = \sigma \boldsymbol{\xi} \quad (5)$$

where $\boldsymbol{\xi}$ is a random symmetric tensor and σ is the strengths of the corresponding noise. The random stress is related to the viscous stress by the fluctuation-dissipation theorem [4]. For incompressible and low-compressible fluids, the covariance of the stress components is:

$$\overline{s^{ik}(\mathbf{r}_1, t_1) s^{lm}(\mathbf{r}_2, t_2)} = \sigma^2 \delta(\mathbf{r}_1 - \mathbf{r}_2) \delta(t_1 - t_2) \\ \sigma^2 = 2\mu k_B T \delta^{im} \delta^{kl}, \quad (6)$$

where k_B is the Boltzmann constant, T denotes the temperature, $\delta(z)$ is the Dirac delta function and δ^{ij} is the Kronecker delta function. In general, the density and viscosity of the fluid are functions of the solute concentration C .

III. SPH DISCRETIZATION

In this work we use a fourth-order weighting function to describe W [9] and obtain the particle number density as

$$\langle \langle n_i \rangle \rangle = \sum_{j=1}^N W(|\mathbf{r} - \mathbf{r}_j|, h), \quad (7)$$

An SPH discretization of the Navier-Stokes Eqs. (1) and (2) can be obtained as:

$$\frac{D(m_i \mathbf{v}_i)}{Dt} = \mathbf{F}_i \quad (8)$$

$$\mathbf{F}_i = - \sum_{j=1}^N \left(\frac{P_j}{n_j^2} + \frac{P_i}{n_i^2} \right) \frac{\mathbf{r}_{ij}}{r_{ij}} \frac{dW(r_{ij}, h)}{dr_{ij}} \\ + \sum_{j=1}^N \frac{5(\mu_i + \mu_j)}{n_i n_j} \frac{(\mathbf{v}_{ij} \cdot \mathbf{r}_{ij})}{r_{ij}^2} \frac{\mathbf{r}_{ij}}{r_{ij}} \frac{dW(r_{ij}, h)}{dr_{ij}} \\ + m_i \mathbf{g} \\ + \sum_{j=1}^N \left(\frac{\mathbf{s}_j}{n_j^2} + \frac{\mathbf{s}_i}{n_i^2} \right) \cdot \frac{\mathbf{r}_{ij}}{r_{ij}} \frac{dW(r_{ij}, h)}{dr_{ij}}. \quad (9)$$

Following [9] and [10] a numerical discretization of the convection-diffusion equation is obtained as

$$\frac{D(m_i C_i)}{Dt} = \sum_{j=1}^N \frac{(D_i^F m_i n_i + D_j^F m_j n_j)(C_i - C_j)}{n_i n_j} \left(\frac{1}{r_{ij}} \frac{dW(r_{ij}, h)}{dr_{ij}} \right). \quad (10)$$

The particle positions are evolved in time according to

$$\frac{d\mathbf{r}_i}{dt} = \mathbf{v}_i. \quad (11)$$

Here, \mathbf{v}_i is the velocity of particle i , t is time, P_i is the fluid pressure at \mathbf{r}_i , \mathbf{s}_i is the random stress at \mathbf{r}_i , $r_{ij} = |\mathbf{r}_{ij}|$, $\mathbf{r}_{ij} = \mathbf{r}_i - \mathbf{r}_j$, and $\mathbf{v}_{ij} = \mathbf{v}_i - \mathbf{v}_j$. For computational efficiency, we set h to unity and locate particles within the interaction range using a common link-list approach with an underlying cubic-lattice of size $h = 1.0$.

To close the system of SPH equations we employ a common equation of state (EOS) in the form

$$P_i = c^2 m_i n_i, \quad (12)$$

where c is the artificial speed of sound, which is chosen such that the desired compressibility of the system is obtained. Depending on application, this EOS is often applied to incompressible systems [11]–[13], where a choice of c , based on dimensionless analysis [14], can yield the quasi-incompressible approximation of an incompressible fluid.

In general, m_i and μ_i depend on C_i . In SPH, the mass fraction can be defined as $\tilde{C}_i = m_i^s / m_i = m_i^s / (m_i^0 + m_i^s)$, where m_i is the total mass of particle i (mass of the solution carried by particle i), m_i^s is the mass of solute, and m_i^0 is the mass of solvent carried by particle i . Then, the dependence of m_i on C_i can be expressed as

$$m_i = m_i^0 + m_i \tilde{C}_i = m_i^0 + m_i C_{max} C_i. \quad (13)$$

In the following we assume that m_i^0 is constant (i.e. does not change as result of diffusion), $\tilde{C} \ll 1$ (dilute solution), the mass of solute carried by particle i is $m_i^s = m_i^0 \tilde{C}_i$ and

$$m_i = m_i^0 + \kappa C_i \quad (14)$$

where $\kappa = m_i^0 C_{max}$ is a constant. Then Eq. (10) can be linearized as

$$\frac{DC_i}{Dt} = \frac{1}{m_i^0} \sum_{j=1}^N \frac{(D_i^F m_i n_i + D_j^F m_j n_j)(C_i - C_j)}{n_i n_j} \left(\frac{1}{r_{ij}} \frac{dW(r_{ij}, h)}{dr_{ij}} \right). \quad (15)$$

For the sake of simplicity we neglect the dependence of the viscosity on the fluid compositions.

In SPH, the fluid domain is discretized with fluid particles with volume $\Delta V_i = 1/n_i$ and time integration is done with

time step Δt . Therefore, we can write the lm -component of the random stress tensor at \mathbf{r}_i as:

$$s_i^{lm} = \sqrt{\frac{2\mu k_B T \delta^{lm}}{\Delta V_i \Delta t}} \xi_i^{lm} = \sqrt{\frac{2\mu k_B T \delta^{lm} n_i}{\Delta t}} \xi_i^{lm}, \quad (16)$$

where ξ_i^{lm} is a unitless random number from a uniform or normal distribution with a unit variance. No summation over repeating indices is assumed in Eq. (16).

In order to maintain the kinetic energy of the modeled system independent of resolution (number of particles), and to recover the appropriate scaling behavior of velocity fluctuations with temperature, we follow the work of [15] and introduce scaling of the Boltzmann constant, k_B . Consider a fluid system modeled with two different resolutions corresponding to N^* and N number of particles, respectively, where N^* is the number of particles in the referenced model. We assume that the Boltzmann constant in the system with N^* particles is k_B , and in the system with N particles is \tilde{k}_B . Equating the total kinetic energy of the models with these two resolutions leads to $\frac{3}{2}N^*k_B T = \frac{3}{2}N\tilde{k}_B T$. Noting that the average volume of particles is inversely proportional to the number of particles we arrive to the scaling law

$$\tilde{k}_B = \frac{V}{V^*} k_B, \quad (17)$$

where V is the average volume of particles in the system with N particles and V^* is the average volume of particles in the system with N^* particles. Next, we rewrite Eq. (16) as

$$s_i^{lm} = \sqrt{\frac{2\mu V^* \tilde{k}_B T \delta^{lm} n_i}{V_i \Delta t}} \xi_i^{lm}, \quad (18)$$

where we replace V with $V_i = 1/n_i$, the volume of particle i . We numerically determined that the correct hydrodynamics is obtained with $V^* = 2h^3$. Therefore, we set the expression for stress to:

$$s_i^{lm} = \sqrt{\frac{4h^3 \mu T^* \delta^{lm} n_i^2}{\Delta t}} \xi_i^{lm}, \quad (19)$$

where $T^* = \tilde{k}_B T$.

To integrate the SPH Eqs. (8) and (11), an explicit ‘‘velocity-Verlet’’ algorithm [16] is employed and time step stability of the solution is ensured by satisfying the time step constraints of [11].

IV. VALIDATION OF THE SPH METHOD FOR LLNS EQUATIONS

We study the accuracy of the SPH solution of the LLNS equations by comparing thermodynamic quantities such as kinetic temperature and velocity variance obtained from the SPH simulations and analytical solutions.

A. Convergence of SPH solution of the LLNS equations

First, we study the convergence behavior of the SPH solution of the stochastic NS equations with respect to spatial resolution. The normalized kinetic temperature $T_{kin}^* = \tilde{k}_B T_{kin}$ is computed as

$$T_{kin}^* = \frac{1}{3} \sum_{i=1}^N m_i (\delta v_{x,i}^2 + \delta v_{y,i}^2 + \delta v_{z,i}^2), \quad (20)$$

where $\delta v_{k,i} = v_{k,i} - \langle v_k \rangle$ ($k = x, y, z$) are the fluctuations of k -component of the velocity of particle i around the mean velocity in k -direction, $\langle v_k \rangle = \frac{1}{N} \sum_{i=1}^N v_{k,i}$. In our simulations there are no sources of energy other than random fluctuations and the kinetic temperature of the system should theoretically be equal to the temperature that is prescribed in Eq. (6), i.e. T_{kin}^*/T^* should be equal to one.

In Fig. 1 we plot T_{kin}^*/T^* versus the equilibrium density n_{eq} . In the simulations shown in this figure, the equilibrium mass density is kept constant ($\rho_{eq} = 30$) and the mass of the particles is set to $m_i = m_0 = \rho_{eq}/n_{eq}$. It is important to note that the speed of sound should scale with mass as

$$c \sim \sqrt{\frac{\tilde{k}_B T}{m_0}} = \sqrt{\frac{2h^3 \rho_{eq} T^*}{m_0^2}}. \quad (21)$$

To obtain this scaling in the SPH model, we start with the expression for the pressure variance derived in [4]:

$$\langle \delta P^2 \rangle = \frac{\rho_{eq} k_B T c^2}{\Delta V}, \quad (22)$$

where δP is the fluctuation of pressure around the mean pressure. Noting that in the above equation $\Delta V = 1/n_{eq}$, $\delta P = c^2 m_i \delta n$ (δn is the fluctuation of density around n_{eq}) and $\rho_{eq} = m_i n_{eq}$ and replacing k_B with \tilde{k}_B we obtain the scaling law for the speed of sound

$$c = \beta \sqrt{\frac{2h^3 \rho_{eq} T^*}{m_0^2}}, \quad (23)$$

where β is the inverse of the coefficient of variation of the particle number density,

$$\beta = \frac{n_{eq}}{\sqrt{\langle \delta n^2 \rangle}}. \quad (24)$$

This results in the EOS

$$P_i = T^* 2h^3 n_{eq} n_i \beta. \quad (25)$$

We numerically determined that to recover the correct hydrodynamic behavior, β should be approximately equal to 5.5. A significantly smaller β results in a high compressibility of the fluid and may lead to numerical instability. For higher β (i.e. for less compressible fluids), the thermodynamic variables become dependent on the speed of sound. Therefore, in all our simulations we set $\beta = 5.5$. Figure 1 shows T_{kin}^*/T^* for $T^* = 0.001, 0.005, 0.01, 0.05$. For all considered temperatures, convergence is reached at a number density of about $n_{eq} = 20$ with the error being less than 2%. Kinetic

temperatures obtained from simulations using an SDPD implementation of the stochastic force are slightly higher with a maximum error of about 4%.

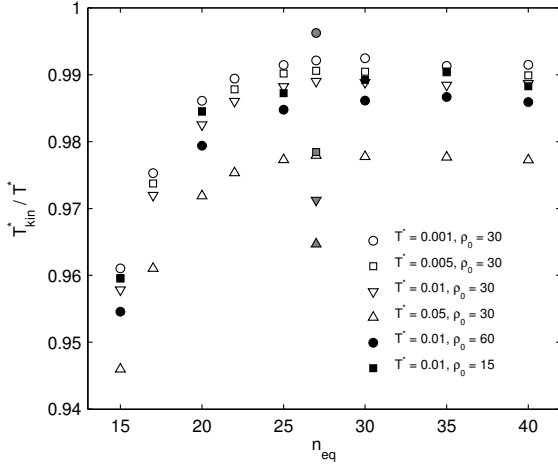


Fig. 1. Scaling of kinetic system temperature with changes in resolution and changes of the mass density ρ_0 where $\mu = 10$. Convergence is reached for $n_{eq} \geq 20$. Gray markers correspond to the kinetic temperatures for the SDPD implementation of the stochastic stress at $n_{eq} = 27$.

It follows from Eq. (20) that for all SPH particles having the same masses $m_i = \rho_0/n_{eq}$, the velocity variance $\sigma_v^2 = \frac{1}{3} \sum_{i=1}^N (\delta v_{x,i}^2 + \delta v_{y,i}^2 + \delta v_{z,i}^2)$ should scale as

$$\sigma_v^2 = \frac{T^*}{m_0} = \frac{n_{eq} T^*}{\rho_0}, \quad (26)$$

i.e. that for a fluid with a given mass density ρ_0 , the velocity variance is inversely proportional to the mass of the SPH particles or linearly proportional to the resolution n_{eq} .

B. Self-diffusion coefficient

The coefficient of mechanical diffusion (describing the "diffusion" of the SPH particles), i.e. the self-diffusion coefficient has a similar scaling behavior as the velocity variance. For example, for an SDPD model with a slightly different discretization of the viscous force than used in this work, the self-diffusion coefficient was obtained as [17]:

$$D = \frac{\tau k_B T}{3} = \zeta \frac{n_{eq} h^2 k_B T}{\mu}, \quad (27)$$

with $\zeta = \frac{1}{12}$. For our SPH model, we numerically determined the value of $\zeta = 0.045$.

To validate the scaling of D , we compute the diffusion coefficient from SPH simulations over the same range of number densities and temperatures as in the previous example.

Figure 2 shows the resulting scaling of the diffusion coefficients with changing resolution, which agrees with Eq. (27).

The same correct linear scaling for the diffusion coefficient is obtained for the whole temperature range considered in the simulations.

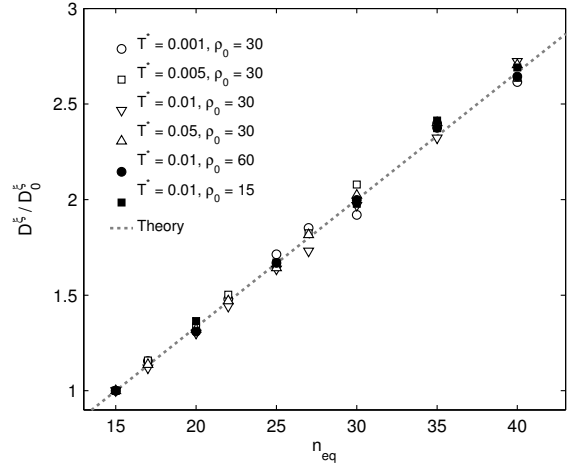


Fig. 2. Scaling of the stochastic diffusion coefficient with increasing resolution, where D_0^ξ is the diffusion coefficient at $n_{eq} = 15$ for each temperature T^* . D^ξ is obtained by linear regression of $\text{MSD}/\Delta t$ where $\text{MSD} > 1.0 h$.

V. SPH MODEL FOR HIGHLY DILUTED SOLUTIONS

Here we study the enhancement of Fickian diffusion by thermal fluctuations in non-equilibrium systems. In this section we study highly diluted solutions. To isolate the effect of stochastic fluxes in Eq. (3) we assume that the advection velocity is zero and only solve Eq. (3). As shown numerically in [18], the effective diffusion coefficient D^{eff} consists of a deterministic Fickian part D^F and a stochastic contribution D^ξ : $D^{eff} = D^F + D^\xi$. In turn, D^ξ is a result of the random advection (which is characterized by the self-diffusion coefficient in Eq. (27)).

In order to study the effect of diffusion enhancement we simulate a spherical plume with radius $3h$ and an initial uniform concentration $C_0 = 1.0$ surrounded by a solution with zero concentration. We run the simulations with four different temperatures ($T^* = 0.001, 0.005, 0.01$ and 0.05), the ratio D^F/D^ξ ranging from 2 – 10 and the value of D^ξ is estimated from Eq. (27).

In order to study the accuracy of the SPH solution of the stochastic and deterministic advection-diffusion equations we solve: (1) the deterministic diffusion equation in the absence of advection; (2) the coupled LLNS and stochastic advection equation ($D^F = 0$); and (3) the coupled LLNS and stochastic advection-diffusion equations. In the first case we compute the resulting diffusion coefficient and compare it with the prescribed Fickian diffusion coefficient. In the second case we numerically compute D^ξ . Once the deterministic solution is verified and D^ξ is evaluated, we compute the effective diffusion coefficient in the third simulation as

$$D^{eff} = D^\xi + D^F \quad (28)$$

and compare this value with the effective diffusion coefficient obtained from the SPH solution of the LLNS and stochastic diffusion equation with the corresponding D^F and T^* .

The results of the simulations indicate a very good agreement between D^{eff} obtained from Eq. (28) and the solution of the full stochastic diffusion equation (see Fig. 3). The relative errors are between 0.8% and 2.5%.

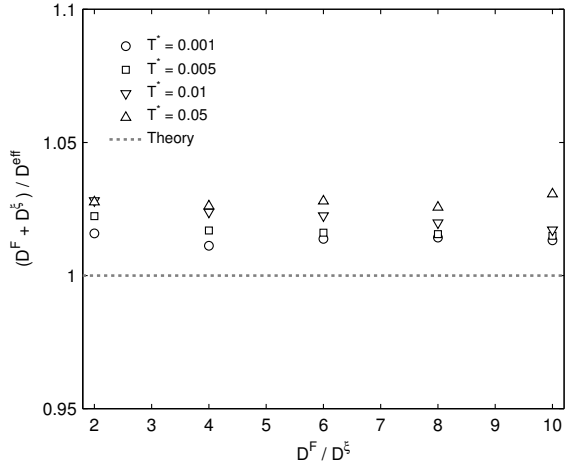


Fig. 3. Accuracy of the diffusion enhancement for different ratios of D^F/D^E . Diffusion coefficients $D^E + D^F$ are obtained from simulations where only Fickian diffusion is active or where only thermal fluctuations occur and then compared to simulations where both are present.

VI. SPH SOLUTION OF THE COUPLED LLNS AND STOCHASTIC DIFFUSION EQUATIONS

Here we use the coupled stochastic SPH model to study the effect of gravity on thermally enhanced diffusive transport. Specifically, we study perturbations of a front between two miscible fluids due to random stresses and fluxes in the momentum and advection-diffusion equations. In the coupled model we solve the LLNS and stochastic advection-diffusion equations with the mass of SPH particles (and density of the solution) depending on C according to Eq. (14).

We simulate a three-dimensional domain filled with the solution of a conservative species C . We consider two cases: (1) initial C is zero in the upper half of the domain and one in the lower half of the domain; and (2) initial C is one in the upper half of the domain and zero in the lower half of the domain. In the first case we use the SPH model to study how gravity suppresses perturbations of the front (also known as giant fluctuations). In the second case we use the stochastic SPH model to study the effect of random stresses and diffusive fluxes on the development of the Rayleigh-Taylor instability.

In both study cases, the domain size is $L_x = L_y = 16h$ and $L_z = 8h$. The upper and lower horizontal boundaries are assumed to be impermeable and all the vertical boundaries are treated as periodic.

The solvent mass for all particles is set to $m_i^0 = m_0 = 1$ and m_i is computed according to Eq. (14). The parameter κ in Eq. (14) is related to the Atwood number, A , via

$$A = \frac{m(C=1) - m(C=0)}{m(C=1) + m(C=0)} = \frac{\kappa}{2m^0 + \kappa}, \quad (29)$$

where $m(C=1)$ and $m(C=0)$ are the masses of particles with $C=1$ and $C=0$, respectively.

A. Giant fluctuations

Here we consider two scenarios: (1) with gravity; and (2) in the absence of gravity. In both scenarios, the solution with $C=0$ (“light fluid”) lies on top of the solution with $C=1$ (“heavy fluid”), the Atwood number is $At = 0.83$ ($\kappa = 10$) and the temperature is set to $T^* = 0.001$. In the first scenario, the system is initially equilibrated, i.e. brought to hydrostatic condition by solving only the NS equations. $C=0$ and 1 are maintained in the upper and lower part of the domain, respectively, during the equilibration process. In the absence of gravity, there is no need to pre-equilibrate the particle system in the simulations of the second scenario. For each scenario we conduct three simulations: (1) no Fickian diffusion, i.e., $D^F = 0.0$; (2) $D^F = 0.001$; and (3) $D^F = 0.005$.

Figure 4 shows the cross-sections of the resulting concentrations at time $t = 414$ for each of the six simulations described above. Subfigures in the top row show the distribution of C obtained from the simulations in the absence of gravity, where one can clearly see the presence of giant fluctuations or perturbations of the front. Subfigures in the bottom row show the distribution of C obtained from the simulations with gravity. It can be seen that gravity significantly reduces front perturbations for all considered values of D^F , but the effect of gravity becomes less pronounced with increasing D^F . As D^F becomes significantly larger than D^E (or when $T^* \rightarrow 0$), the stochastic diffusion reduces to a deterministic diffusion and thus fluctuations completely disappear.

1) *Structure factor*: In the absence of gravity, the nonequilibrium concentration fluctuations are known to exhibit a characteristic q^{-4} decay of the powerspectrum [19]. However, this can only be observed over a limited range of wavenumbers due to several effects that relax the fluctuations and eliminate the scale-invariant character. At low wavenumbers the primary reason is a finite size of the domain [20]. Gravity dampens the fluctuations leading to a much weaker dependence of the power spectrum on wavenumber [21].

We obtain the power spectrum $S(q)$ from simulations similar to the ones described in Sec. VI with the domain size $L_x = L_y = 32h$ and $L_z = 16h$, temperature $T^* = 0.003$ (which corresponds to a Schmidt number of $Sc \approx 1000$), $\kappa = 10$. In these simulations, the light fluid ($C=0$) lies on top of the heavy fluid ($C=1$). According to [22], in the absence of gravity the scale-invariant characteristics of the power spectrum are independent of the fluid configuration and concentration gradient and scale as

$$S(q)/S^\infty = (q^4 + Bq^2 + \Lambda^4)^{-1}. \quad (30)$$

Here $B = \Lambda \tanh(\Lambda/2) [2\Lambda \tanh(\Lambda/2) - 4]$ and Λ is a fitting constant. To normalize the data, the asymptotic value of $S^\infty = \lim_{q \rightarrow \infty} S(q)q^4$ is obtained from a fit of the linear part of $S(q)q^4$ which corresponds to fitting a power-law function $S^\infty q^{-4}$ to $S(q)$.

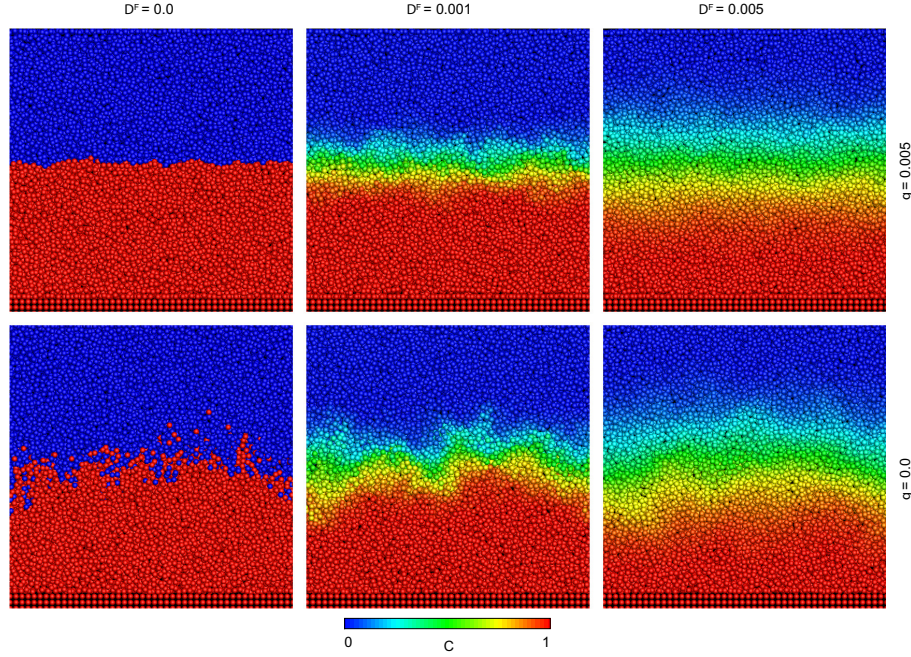


Fig. 4. Cross-section of the interface between a heavy fluid and a light fluid on top at time $t = 414$. Temperature is $T^* = 0.001$, $\kappa = 10$, $\mu = 10$. (Upper row) In the presence of gravity with same increase of Fickian diffusion from left to right. (Lower row) Without gravity and increasing Fickian diffusion from left to right.

Figure 5 shows the resulting power spectra scaled onto the universal curve according to Eq. (30) with $\Lambda = 2.33$ and the theoretical scaling for bounded and unbounded conditions. This confirms the scale-invariant nature of the fluctuation front and the saturation due to finite-size effects at low wave numbers. The power spectrum of the interface in the presence of gravity clearly shows the saturation of the divergence at low wave numbers.

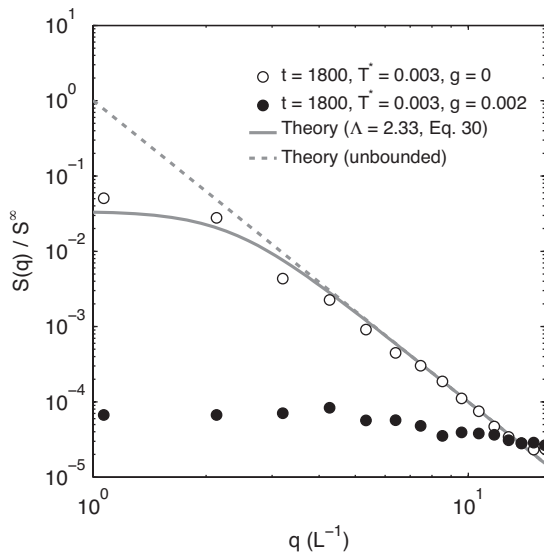


Fig. 5. Power spectra obtained from the remapped concentration fields at $t = 1800$ including the effect of gravity.

B. Rayleigh-Taylor instability

Here we study the effect of thermal fluctuations on the development of the Rayleigh-Taylor instability, an unstable displacement of a light ($C=0$) fluid with a heavy fluid ($C=1$) under the action of gravity. In the considered cases, the Atwood number is $A = 0.6$ ($\kappa = 3$), gravity is $g = 0.002$, viscosity is $\mu = 10$ and the number density is $n_{eq} = 27$. The domain size is $L_x = 16h$, $L_y = 8h$ and $L_z = 32h$. The no-flow boundary condition is imposed in the z direction by placing a layer of boundary particles at the bottom of the domain. Periodic boundary conditions are imposed in the x and y directions. To initiate the Rayleigh-Taylor instability we perturb the interface according to

$$z(x) = z_0 + \cos(\pi x/L_x)\eta_0, \quad (31)$$

where $z_0 = 0.5L_z + 1$ with the initial amplitude $\eta_0 = 0.5$ and the wavelength $\lambda = 16h$.

This yields a pseudo-2D simulation setup. In order to bring the system to a hydrostatic equilibrium we solve the LLNS equations including thermal fluctuations (no Fickian diffusion) and constantly reassign the appropriate concentrations above and below the interface defined by Eq. (31). In the final simulations we investigate three cases with the same effective diffusion coefficient $D^{eff} = 0.00036$ ($Sc \approx 1000$): (1) $D^\xi = 0.00012$, $D^F = 0.00024$, (2) $D^\xi = 0$, $D^F = 0.00036$ and (3) $D^\xi = 0.00012$, $D^F = 0.00024$ to compare the time evolution of the diffusive interface.

Figure 6 shows the resulting evolution of the unstable front and Fig. 7 displays the corresponding interface amplitude for

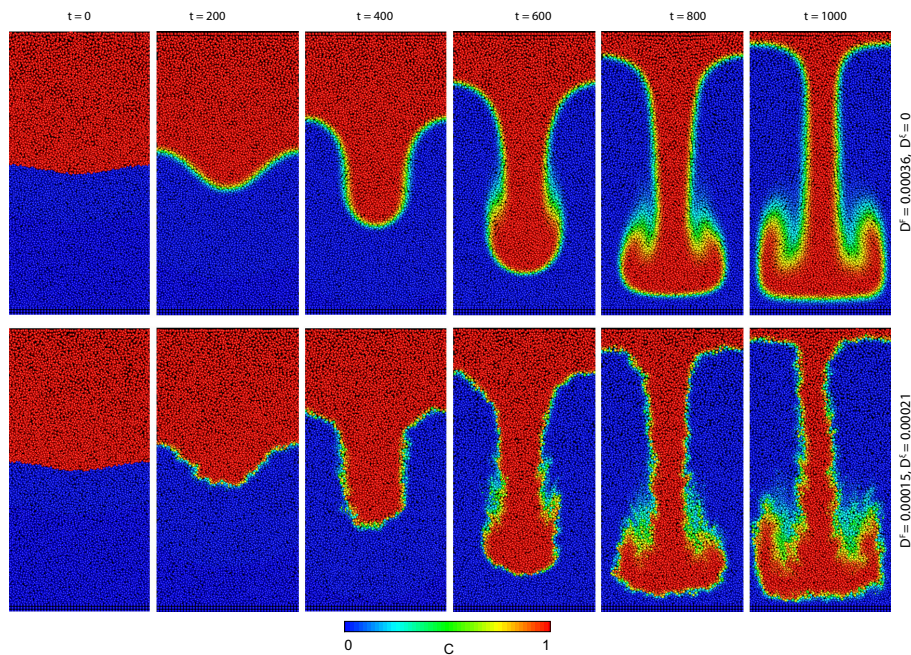


Fig. 6. Rayleigh-Taylor instability at a Schmidt number of $Sc \approx 1000$ ($D^{eff} = 0.00036$), $At = 0.6$ ($\kappa = 3$), gravity $g = 0.002$, viscosity $\mu = 10$ and number density $n_{eq} = 27$. Domain size is $L_x = 16h$, $L_y = 8h$ and $L_z = 32h$. (Upper row) Only fickian diffusion with $D^F = 0.00036$. (Lower row) $D^F = 0.00024$ and $D^S = 0.00012$, $T^* = 0.002$.

both the stochastic and deterministic cases. In general, both solutions agree well with the analytical solutions of [23] and [24] for early times ($t \lesssim 300$) and with the late time behavior given by [25] ($t \gtrsim 300$), where $a_q = 0.035$. This is in agreement with the wide range of a_q values that have been reported in literature [26] and lie between 0.01 and 0.08. Figure 7 (right panel) shows that the front in the stochastic simulation propagates faster, especially at late times. The rate of the front perturbation growth is proportional to the concentration time. The coefficient of Fickian diffusion is smaller in the stochastic model ($D^F < D^{eff}$) than in the deterministic model ($D^F = D^{eff}$) and, as a result, the concentration gradients across the interface are higher in the stochastic simulation than in the deterministic simulation, which can be seen in Fig. 6. Therefore, the front perturbation grows faster in the stochastic simulation than in the deterministic simulation. Simulations using the SDPD implementation display a slightly slower development of the front growth at late times compared to the LLNS-SPH simulations. This is most likely caused by the difference in kinetic temperatures (about 4%, see Fig. 1) as development of vortices rolled up along the tail is favored and thus leading to higher drag forces on the perturbation front at late times.

VII. CONCLUSION

We presented a novel, Smoothed Particle Hydrodynamics based, method for solving coupled LLNS and stochastic advection-diffusion equations. It is shown that the resulting stochastic SPH model produces a correct scaling behavior of thermodynamic quantities, such as velocity variance and

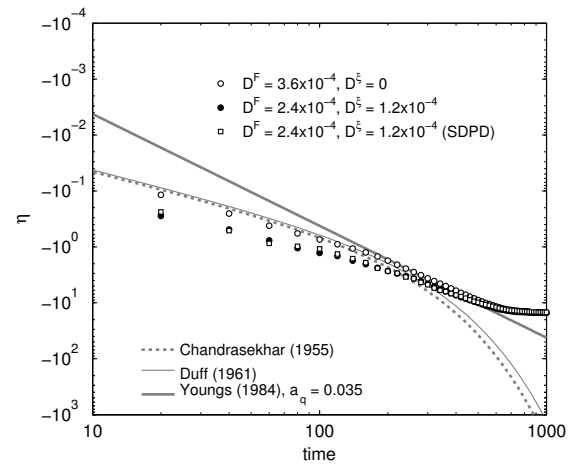


Fig. 7. Simulations of the Rayleigh-Taylor instability with same effective diffusion $D^{eff} = 0.00036$ at Schmidt number $Sc \approx 1000$ and $g = 0.002$ and the corresponding simulations using the SDPD implementation. The solution of [23] and [24] have been derived for early times. In contrast the analytical solution of [25] is valid for late times and employs the α_q calibration parameter which has been reported by various lab and numerical experiments to lie in a range between 0.01 and 0.08 [26] (here $a_q = 0.035$).

self-diffusion coefficient. To investigate the effect of thermal fluctuations on diffusive mixing we (1) simulated diffusion of a plume and demonstrated the accuracy of the SPH model with an error of less than 2%. (2) The role of thermal fluctuations on the evolution of a diffusive interface between a light fluid lying on top of a heavy fluid has been demonstrated. In agreement with recent laboratory experiments and theoretical consider-

ations, we demonstrated (3) that in the absence of gravity the SPH model recovers the characteristic q^{-4} divergence of the interface power spectrum and its scale-invariant nature. Also in agreement with previous studies, our results show that gravity reduces the perturbations of the miscible front. Lastly (4), we used the stochastic SPH model to study the effect of thermal fluctuations on the development of the Rayleigh-Taylor instability. We found that random thermal fluctuations slightly accelerate the development of the instability. In the stochastic SPH model, mixing of two miscible fluids results from mechanical mixing of two fluids due to random advection and diffusive mixing. In the standard deterministic description (based on the Navier-Stokes and advection-diffusion equation) the mixing is treated as an effective diffusion process. Therefore, the deterministic model produces smaller concentration gradients across the front separating two miscible fluids, which slows the development of the Rayleigh-Taylor instability.

ACKNOWLEDGMENT

This work was partially supported by the DAAD (German Academic Exchange Service) providing J. Kordilla with an international research scholarship at the Pacific Northwest National Laboratory (PNNL), USA. A.M. Tartakovsky was supported by the Department of Energy's Office of Advanced Scientific Computing Research Program and at Pacific Northwest National Laboratory (PNNL). PNNL is operated by Battelle for the U.S. Department of Energy. W. Pan was supported by the Applied Mathematics Program within the U.S. Department of Energy Office of Advanced Scientific Computing Research as part of the Collaboratory on Mathematics for Mesoscopic Modeling of Materials (CM4), under award number DE-SC0009247.

REFERENCES

- [1] J. Bear, *Dynamics of fluids in porous media*. Courier Dover Publications, 1972.
- [2] A. Fick, "Ueber Diffusion," *Annalen der Physik*, vol. 170, no. 1, pp. 59–86, 1855. [Online]. Available: <http://onlinelibrary.wiley.com/doi/10.1002/andp.18551700105/abstract>
- [3] A. Vailati and M. Giglio, "Giant fluctuations in a free diffusion process," *Nature*, vol. 390, no. November, pp. 4–7, 1997.
- [4] L. D. Landau and E. M. Lifshitz, *Fluid Mechanics: Volume 6 (Course Of Theoretical Physics)*. Butterworth-Heinemann, 1987.
- [5] M. Serrano and P. Español, "Thermodynamically consistent mesoscopic fluid particle model," *Physical Review E*, vol. 64, no. 4, p. 046115, Sep. 2001. [Online]. Available: <http://link.aps.org/doi/10.1103/PhysRevE.64.046115>
- [6] A. Ladd, "Short-time motion of colloidal particles: Numerical simulation via a fluctuating lattice-Boltzmann equation," *Physical Review Letters*, vol. 70, no. 9, pp. 1339–1342, Mar. 1993. [Online]. Available: <http://link.aps.org/doi/10.1103/PhysRevLett.70.1339>
- [7] P. Español, M. Serrano, and H. Öttinger, "Thermodynamically Admissible Form for Discrete Hydrodynamics," *Physical Review Letters*, vol. 83, no. 22, pp. 4542–4545, Nov. 1999.
- [8] M. Grmela and H. Öttinger, "Dynamics and thermodynamics of complex fluids. I. Development of a general formalism," *Physical Review E*, vol. 56, no. 6, p. 6620, 1997. [Online]. Available: http://pre.aps.org/abstract/PRE/v56/i6/p6620_1
- [9] A. Tartakovsky and P. Meakin, "A smoothed particle hydrodynamics model for miscible flow in three-dimensional fractures and the two-dimensional Rayleigh-Taylor instability," *Journal of Computational Physics*, vol. 207, pp. 610–624, 2005.
- [10] Y. I. Zhu and P. J. Fox, "Simulation of Pore-Scale Dispersion in Periodic Porous Media Using Smoothed Particle Hydrodynamics," *Journal of Computational Physics*, vol. 182, no. 2, pp. 622–645, 2002. [Online]. Available: <http://linkinghub.elsevier.com/retrieve/pii/S0021999102971895>
- [11] J. P. Morris, "Modeling Low Reynolds Number Incompressible Flows Using SPH," *Journal of Computational Physics*, vol. 136, no. 1, pp. 214–226, Sep. 1997.
- [12] A. Tartakovsky and P. Meakin, "Modeling of surface tension and contact angles with smoothed particle hydrodynamics," *Physical Review E*, vol. 72, p. 026301, 2005.
- [13] J. Kordilla, A. Tartakovsky, and T. Geyer, "A Smoothed Particle Hydrodynamics model for droplet and film flow on smooth and rough fracture surfaces," *Advances in Water Resources*, vol. 59, pp. 1–14, May 2013. [Online]. Available: <http://linkinghub.elsevier.com/retrieve/pii/S0309170813000729>
- [14] J. J. Monaghan, "Smoothed particle hydrodynamics," *Annual Review of Astronomy and Astrophysics*, vol. 68, pp. 543 – 574, 1992.
- [15] R. M. Fuchsliin, H. Fellermann, A. Eriksson, and H.-J. Ziock, "Coarse-Graining and Scaling in Dissipative Particle Dynamics," *The Journal of Chemical Physics*, p. 8, Mar. 2007.
- [16] M. Allen and D. Tildesley, *Computer Simulation of Liquids*. Clarendon Press, Oxford, 1989.
- [17] S. Litvinov, M. Ellero, X. Hu, and N. A. Adams, "Self-diffusion coefficient in smoothed dissipative particle dynamics," *The Journal of chemical physics*, vol. 130, no. 2, p. 021101, Jan. 2009.
- [18] A. Donev, J. B. Bell, A. de la Fuente, and A. Garcia, "Diffusive Transport by Thermal Velocity Fluctuations," *Physical Review Letters*, vol. 106, no. 20, p. 204501, May 2011. [Online]. Available: <http://link.aps.org/doi/10.1103/PhysRevLett.106.204501>
- [19] T. Kirkpatrick, E. Cohen, and J. Dorfman, "Light scattering by a fluid in a nonequilibrium steady state. II. Large gradients," *Physical Review A*, vol. 26, no. 2, 1982. [Online]. Available: http://pra.aps.org/abstract/PRA/v26/i2/p995_1
- [20] A. Vailati, R. Cerbino, S. Mazzoni, M. Giglio, G. Nikolaenko, C. J. Takacs, D. S. Cannell, W. V. Meyer, and A. E. Smart, "Gradient-driven fluctuations experiment: fluid fluctuations in microgravity," *Applied optics*, vol. 45, no. 10, pp. 2155–65, Apr. 2006. [Online]. Available: <http://www.ncbi.nlm.nih.gov/pubmed/16607979>
- [21] A. Vailati, R. Cerbino, S. Mazzoni, C. J. Takacs, D. S. Cannell, and M. Giglio, "Fractal fronts of diffusion in microgravity," *Nature communications*, vol. 2, p. 290, Jan. 2011.
- [22] J. M. Ortiz de Zárate, F. Peluso, and J. V. Sengers, "Nonequilibrium fluctuations in the Rayleigh-Benard problem for binary fluid mixtures," *The European physical journal. E, Soft matter*, vol. 15, no. 3, pp. 319–33, Nov. 2004. [Online]. Available: <http://www.ncbi.nlm.nih.gov/pubmed/15592772>
- [23] S. Chandrasekhar, "The character of the equilibrium of an incompressible heavy viscous fluid of variable density," *Mathematical Proceedings of the Cambridge Philosophical Society*, vol. 51, no. 01, p. 162, Oct. 1955. [Online]. Available: http://www.journals.cambridge.org/abstract_S0305004100030048
- [24] R. E. Duff, F. H. Harlow, and C. W. Hirt, "Effects of Diffusion on Interface Instability between Gases," *Physics of Fluids*, vol. 5, no. 4, p. 417, 1962. [Online]. Available: <http://link.aip.org/link/PFLDAS/v5/i4/p417/s1&Agg=doi>
- [25] D. L. Youngs, "Numerical simulation of turbulent mixing by Rayleigh-Taylor instability," *Physica D: Nonlinear Phenomena*, vol. 12, no. 1-3, pp. 32–44, Jul. 1984. [Online]. Available: <http://linkinghub.elsevier.com/retrieve/pii/0167278984905128>
- [26] J. Glimm, J. Grove, X. Li, W. Oh, and D. Sharp, "A Critical Analysis of RayleighTaylor Growth Rates," *Journal of Computational Physics*, vol. 169, no. 2, pp. 652–677, May 2001.